Growing up in the city : a study of galaxy cluster progenitors at z>2

Kuiper, E.

6

Dissecting the light from high redshift radio galaxies

We present deep multicolour Hubble Space Telescope images of two powerful $z \sim 2.5$ radio galaxies, MRC 0406-244 and TX 0828+193, that appear to be undergoing active galactic nucleus (AGN) feedback. These galaxies consist of several clumps and filaments that extend for tens of kpc along the radio jets. We decompose the emission into several components and find that the extended emission seems to result from scattered AGN light, nebular emission and possibly from ultraviolet light from young stars and is likely to last only as long as the lifetime of the radio source (10 Myr). In each case the red, and likely older, stellar population is concentrated in a single central region that is not elongated along the radio jet axis. The lack of a disturbed morphology in the red stellar population suggests that no major merger has taken place on the timescale of the young radio emission ($\sim$ 10 Myr). The galaxies have optical half-light radii of $r_e \sim 2 - 3$ kpc and thus are similar in size to other massive high redshift galaxies. If the scattered AGN and nebular light are not removed from the rest-frame optical images, then the effective radii increase by 65%, and the radio galaxies appear larger than typical high redshift galaxies of similar mass. Therefore, beneath the illuminated extended material, these radio galaxies appear to have similar sizes and reside in similar environments as other massive high redshift galaxies.

N. A. Hatch, E. Kuiper, G. K. Miley, H. J. A. Röttgering, C. De Breuck, H. Ford, J. D. Kurk, R. A. Overzier, J. Schaye, B. P. Venemans, A. W. Zirm.
To be submitted to the *Monthly Notices of the Royal Astronomical Society.*

6.1 Introduction

High redshift radio galaxies (HzRGs) are among the brightest known galaxies in the early Universe and are unique laboratories for studying massive galaxy formation. However, many of their properties appear to differ from other distant massive galaxies. HzRGs appear larger than passive or sub-milimetre galaxies at the same redshift (Targett et al. 2011). They comprise several clumps extending over tens of kpc in both the rest-frame ultraviolet (UV) and optical (e.g. Pentericci et al. 1999, 2001), and their extended emission is often aligned with the radio jets (McCarthy et al. 1987; Chambers et al. 1987). HzRGs are usually surrounded by giant Lyα halos of hot gas that can extend for hundreds of kiloparsecs.

The properties of HzRGs, and the fact that several are located within protoclusters (Venemans et al. 2007), led to the suggestion that these galaxies are the progenitors of brightest cluster galaxies (Miley & De Breuck 2008) and are thus a separate population to other massive galaxies. However, since these galaxies are caught in a short-lived but very luminous phase of AGN activity, their morphology and other properties may be distorted by this activity.

The Spiderweb galaxy (MRC 1138-262) at $z = 2.2$ is a powerful HzRG that differs from other massive galaxies at the same epoch. It resides in one of the densest $z > 2$ protoclusters (Kurk et al. 2000), it is surrounded by tens of galaxies that could merge with it or form an extended cD halo (Miley et al. 2006; Hatch et al. 2009), and it is bathed in diffuse UV light emitted from young intergalactic stars (Hatch et al. 2008). The galaxy is caught undergoing a dramatic feedback episode in which a significant fraction of the ambient gas in its halo could become unbound (Nesvadba et al. 2006). Cosmological simulations suggest these feedback episodes in the early Universe may play an important role in galaxy evolution (Croton et al. 2006). But are these extreme feedback episodes limited to a special population of brightest cluster galaxy progenitors, such as the Spiderweb galaxy, or do they affect other populations with properties more typical of massive distant galaxies?

We selected two massive HzRGs (MRC 0406-244 and TX 0828+193) at $z \sim 2.5$ that consist of multiple components aligned with the radio jets, which are also undergoing similarly powerful feedback episodes (Nesvadba et al. 2008). Using deep high-resolution optical and near-infrared Hubble Space Telescope (*HST*) images, we have decomposed the light from these galaxies into their constituent parts: scattered AGN light, nebular emission, and light from the blue and red stellar populations, in order to determine whether HzRGs are a special population, or normal massive galaxies undergoing a special event.

6.2 Observations

Deep images of MRC 0406-244 and TX 0828+193 were obtained with the Advance Camera for Surveys (ACS) and the Wide Field Camera 3 (WFC3) on board the Hubble Space Telescope (*HST*). A single $3.5' \times 3.4'$ ACS and $2.3' \times 2.1'$ WFC3 field

was observed for each HzRG through the optical filters F606W (R_{606}) and F814W (I_{814}) with ACS, and near-infrared filters F110W (J_{110}) and F160W (H_{160}) with WFC3. The total exposure time was 1 orbit in the J_{110} and H_{160} filters (2612 seconds), and 4 orbits in the R_{606} and I_{814} filters (10173 seconds). The exception was the H_{160} image of TX 0828+193, which suffered from strong persistence, due to an earlier observation of Omega Cen, and so was re-observed. The total exposure time of the TX 0828+193 H_{160} image was 2 orbits. The observations were reduced using the PYRAF task MULTIDRIZZLE to produce cosmic-ray removed, registered images. Images were corrected for Galactic extinction using a Calzetti extinction law and $E(B-V) = 0.053$ mag for MRC 0406-244 and $E(B-V) = 0.035$ mag for TX 0828+193.

To examine the environment of the HzRGs, a comparison control field was compiled from 4 separate J_{110} and H_{160} images of the Subaru Deep Field obtained with program 11149 (PI Egami). $H-$band selected catalogues of the HzRG and control fields were created using SExtractor (Bertin & Arnouts 1996) in double image mode. A detection was defined as a minimum of 5 adjacent pixels exceeding the 3σ noise. With these detection parameters we found that the catalogues were 85% complete to $H = 26$ mag. Colours were measured in circular apertures with a $1.6''$ diameter and total magnitudes were measured using SExtractor's MAG_AUTO apertures. The edges, bright stars and diffraction spikes were masked to avoid spurious sources and incorrect photometry. After masking, the area covered was approximately ~ 4.3 arcmin^2 for each HzRG fields, and ~ 17.2 arcmin^2 for the control field.

In Sect. 6.3.2 the I_{814} images are subtracted from the H_{160} images. Therefore the I_{814} images were convolved to match the point spread function (PSF) of the H_{160} images using convolution kernels determined with the IRAF task PSFMATCH. High frequency noise was removed from the PSF matching function by applying a cosine bell taper. The resulting growth curves of stars in the images matched to within 2 per cent at all radii.

6.3 Results

6.3.1 Colour images

Three-colour [R_{606}, J_{110}, H_{160}] images of the radio galaxies are shown in Figure 6.1. MRC 0406-244 comprises several large clumps and filaments extending approximately 36 kpc ($4.4''$) along the same orientation as the radio jets. There is a strong asymmetry in the colour of the northern and southern extensions. TX 0828+193 consists of 5 bright knots lying approximately north-south, in the same orientation as the radio jets. Two diffuse twisted filaments extend north from the top of the northern-most knot. The emission has a total extent of 28 kpc ($3.4''$). The filaments are most pronounced in R_{606} and J_{110}, suggesting that they consist primarily of nebular emission (see Sect. 6.3.2). One of the central knots has a red colour (prominent in H_{160}). The other knots are dominated by bluer emission, of

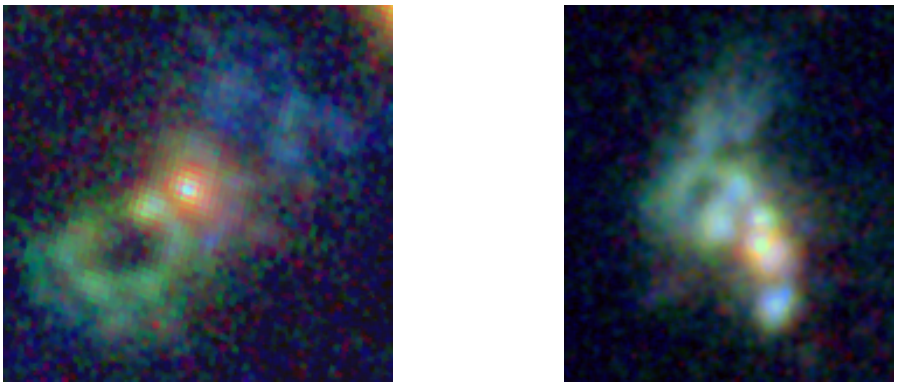

Figure 6.1 – False colour images of MRC 0406-244 (left) and TX 0828+193 (right). The colours are blue – R_{606}, green – J_{110} and red – H_{160}, and the images are $5.0'' \times 4.8''$ (41×40 kpc) and $4.3'' \times 4.8''$ (35×39 kpc), respectively. The yellow object at the top right of the MRC 0406-244 image is a foreground galaxy that is not part of MRC 0406-244.

similar colour to the filaments, suggesting the same processes are involved in their illumination.

6.3.2 Decomposing the light from HzRGs

In the following section we use the available data to estimate the respective contributions of different emission mechanisms. The emission line contribution within each filter was calculated using the long-slit spectroscopy of Taniguchi et al. (2001); Vernet et al. (2001); Iwamuro et al. (2003) and Humphrey et al. (2007). Nebular continuum contribution was calculated with the DIPSO STARLINK code NEBCONT using the Hβ flux, and assuming an electron density of 500 cm^{-3} and a temperature of 1100 K (Nesvadba et al. 2008). Table 6.1 lists the amount of light contributed by nebular emission (both line and continuum) within each observed filter. The uncertainties were minimised where possible by taking continuum and line fluxes from the same slit. However, this was not possible for the R_{606} and I_{814} bands of MRC 0406-244 where instead the continuum was measured directly from the *HST* images from an area matched to the slit size. Furthermore, the nebular contributions quoted are integrated across the slits and there are likely to be significant variations across the HzRGs.

We note that the nebular emission contributions for MRC 0406-244 listed in Table 6.1 are significantly larger than those reported by Rush et al. (1997) who performed a similar study. Based on a composite radio galaxy spectrum they reported contributions of 12, 2.5 and 7 per cent to their r, i and J bands with an uncertainty as high as a factor 2. The difference is likely caused by the much improved data that is used in this work to calculate the nebular emission contributions.

Table 6.1 – Contribution from nebular emission (continuum and line). [1]Only nebular continuum. Nebular line contribution in this filter will be of the order a few per cent.

Band	TX 0828+193	MRC 0406-244	Contributing emission lines
R_{606}	34%	62%	HeII1640, CIV 1550, CIII] 1909, OIII] 1663
I_{814}	24%	33%[1]	CII] 2326, [NeIV] 2429, [OII] 2471
J_{110}	39%	45%	MgII 2798, [NeV] 3426, [OII]3727, [NeIII] 3869
H_{160}	31%	23%	Hγ 4363, HeII 4686, Hβ 4861 (MRC 0406-244 only)

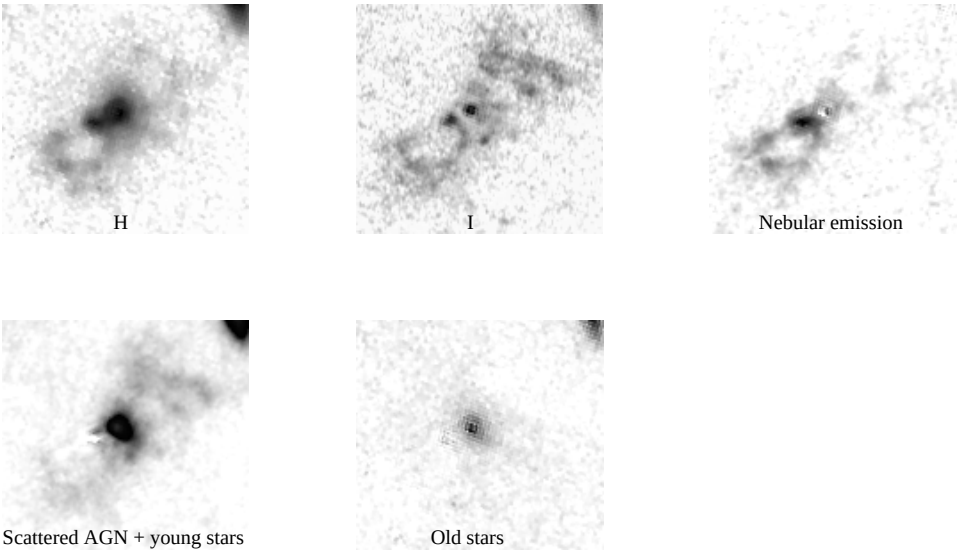

Figure 6.2 – Decomposing MRC 0406-244 into its separate components: *HST* H_{160} (WFC3) and I_{814} images, nebular emission (as traced by [OIII]), scattered AGN light and young stars, and old stars. The old stars are concentrated in a central galaxy, whilst the nebular emission, scattered AGN light and light from the young stars are more extended and aligned along the radio jet axis.

6.3.2.1 MRC 0406-244

Nebular emission: MRC 0406-244 was observed through the H_{160} filter with WFC3 (first panel of Fig. 6.2) and has previously been observed with NICMOS (Pentericci et al. 2001). The NICMOS-F160W filter is marginally wider than the WFC3 H_{160} filter so it also encompassed the bright [OIII] doublet at 4959/5007 Å. Subtracting the WFC3 emission from the NICMOS image therefore shows the exact distribution of [OIII] emission.

Details on the reduction of the NICMOS image can be found in Pentericci et al. (2001). The NICMOS image was registered and flux calibrated to match the WFC3 image using 6 nearby objects visible in both images. We could not apply a PSF

correction as there were no stars in the NICMOS images to measure the PSF. The resulting image showing the distribution of the [OIII] emission is displayed in the third panel of Fig. 6.2. The [OIII]/Hβ ratio is fairly constant across the entire galaxy (Humphrey et al. 2009) so this image also shows the distribution of Hβ and nebular continuum within MRC 0406-244.

Scattered AGN light and young stars: The I_{814} image, shown in the 2nd panel of Fig. 6.2, shows rest-frame $\sim$ 2300 Å emission and hence it potentially contains nebular emission, scattered AGN light, and UV light from young stars. Most of the nebular emission in the I_{814} band is due to nebular continuum since the CII], [NIV] and [OII]2471 Å lines are relatively weak, contributing only a few percent of the emission in the I_{814}-band. Thus, the distribution of nebular emission in this image is likely to be similar to the [OIII] emission. To remove the nebular component, the nebular emission image was scaled to 33% of the I_{814} flux and subtracted from the I_{814}-band image.

The resulting image, displayed in the 4th panel of Fig. 6.2, indicates the distribution of scattered AGN light and young stars. Unfortunately, we are unable to directly distinguish between these two sources of emission. However, the morphology of the residual I_{814} emission resembles a biconical shape, suggesting the extended UV emission is due to scattered AGN light rather than young stars. Furthermore, the residual I_{814} emission does not resemble that of the nebular emission, as would be expected if both resulted from ionization by young stars. Dust extinction may reduce the UV light with respect to the nebular emission, but the northwest extension is brighter in UV relative to the nebular emission, so this cannot be caused by reddening.

Red stellar population: The H_{160} band covers emission from just beyond rest-frame 4000 Å, so it also traces light from both the old and young stellar populations, as well as nebular emission and scattered AGN light. The nebular emission was removed by scaling the [OIII] image to 23% of the H_{160} band flux and then subtracting it from the H_{160} image.

Scattered AGN light was removed by subtracting a scaled version of the residual I_{814} image. Grey-scattered AGN light will have a spectral energy distribution (SED) that is similar to the quasar spectrum. Dust-scattered quasar light and light from unobscured young stellar populations have bluer SEDs between 2300 Å and 4000 Å than the average quasar. We can thus estimate the maximum amount of scattered light and young population by assuming that all the light from the residual-I_{814} images comes from grey-scattered quasar light. The average quasar SED has a relative I_{814}-to-H_{160} flux of 2.83 determined from the spectrum of Vanden Berk et al. (2001). If the residual-I_{814} light is primarily due to a young stellar population or dust scattered quasar light, then we may oversubtract the contribution to the H_{160} images. We check this possibility in Sect. 6.3.2.3.

The location of the red stellar population is shown in the fifth panel of Fig. 6.2.

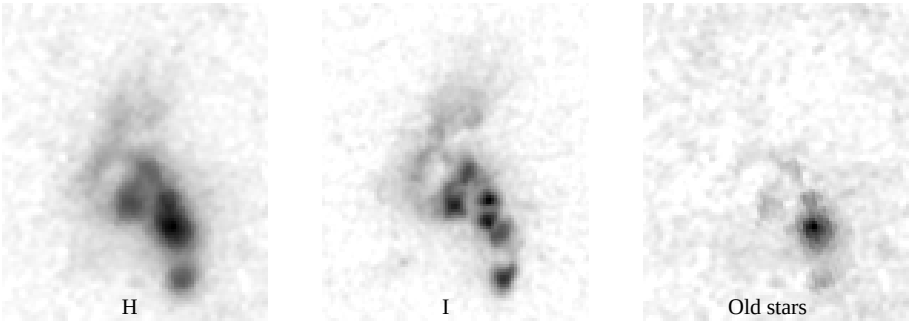

Figure 6.3 – Decomposing TX 0828+193: original *HST* H_{160} and I_{814} images and red stellar population. The residual H-band light (right panel) is concentrated in a central clump corresponding to the brightest knot in the H-band image.

Red stellar populations are often interpreted as being old with little to no ongoing star formation, but may also be young stars that are heavily obscured. The red light originates from a single nuclear region with a regular ellipsoidal morphology. There is no extension along the radio jet axis and the red population shows no signs of tidal features that would have suggested a recent disturbance that may be caused by a major merger.

6.3.2.2 TX 0828+193

Fig. 6.3 displays the H_{160} and I_{814} *HST* images and the rest-frame optical emission from the underlying red stellar population.

Red stellar population: Unfortunately, we cannot determine the distribution of nebular emission as we do not have the appropriate data. However, this galaxy does not display a strong variation in colour, except for the central red knot. The outer parts of the galaxy have similar colours, and Humphrey et al. (2007) report that the spatial distribution of the continuum and emission lines are similar across their long-slit spectra. We thus assume that the distribution of the nebular emission is similar to the continuum in each band, and that the emission in the I_{814} image displays the distribution of the scattered AGN light and young stars.

To obtain the distribution of the red, and possibly old, stellar population, the nebular emission was removed from the H_{160} and I_{814} images by scaling the respective images by the amounts given in Table 6.1. Scattered AGN and young star light was removed by subtracting a scaled version of the I_{814} image from the H_{160} image, assuming the same relative I_{814}-to-H_{160} flux of 2.83 as for MRC 0406-244.

The red stellar population is concentrated into a single clump containing 65% of the residual H_{160} light. The other 4 bright knots have SEDs that are almost entirely consistent with nebular emission and scattered AGN light, although some of the UV light may also be due to a young stellar population.

6.3.2.3 Mass of red stellar population

The residual-H_{160} light shown in the right panels of Figs. 6.2 and 6.3 is greatly reduced compared to the original H_{160} images. To check that we have not over-subtracted light from the H_{160} images, we compare the luminosity derived from the residual H_{160} band images to the expected luminosity from the HzRGs given their large stellar masses determined from Spitzer IRAC measurements (i.e. rest-frame 1.6μm light). Seymour et al. (2007) derive a mass of 2.4×10^{11} $M_\odot$ for MRC 0406-244 and obtain an upper limit of 4×10^{11} $M_\odot$ for TX 0828+193, but De Breuck et al. (2010) show that the typical mass of a HzRG is approximately 2×10^{11} $M_\odot$, so for simplicity we assume that TX 0828+193 has the same mass as that of MRC 0406-244. TX 0828+193 has 23.1 mag of residual H_{160} light and MRC 0406-244 has 22.4 mag of residual H_{160} light.

Based on Bruzual & Charlot (2003) stellar synthesis models, a $z = 2.5$ galaxy of 2.4×10^{11} $M_\odot$ may have an observed H_{160} magnitude in the range of $20 - 25$ mag_{AB} depending on dust content and the age of the stellar population. We model the HzRGs as galaxies with exponentially declining star formation histories with $\tau = 1$ Gyr, that started to form stars prior to $z = 2.5$. Assuming this model, a 2.4×10^{11} $M_\odot$ galaxy will have an observed H_{160} magnitude of 23 mag if it contains enough dust to extinguish the light by $A_V = 1 - 1.5$ mag. Nesvadba et al. (2008) measure $A_{H\beta} = 1 - 4$ mag in these HzRGs, so the residual H_{160} luminosities in Figs. 6.2 and 6.3 are more than sufficient to account for an old stellar population of a few $\times 10^{11}$ $M_\odot$.

6.3.3 Sizes of HzRGs

It has been suggested that radio galaxies at $z > 2$ have larger sizes than normal massive galaxies or sub-mm galaxies (Targett et al. 2011). However, Figs. 6.2 and 6.3 show that much of the extended light above 4000 Å is due to nebular emission, scattered quasar light and young stars. Hence the sizes of the galaxies, as measured from the red stellar population, are likely to be smaller than those measured from the original H_{160} images.

An ellipsoid model was fit to the H_{160} and residual-H_{160} images of each HzRG. Since the galaxies do not have regular Sersic profiles, we did not fit a galaxy model to the profiles, but instead determined the circularised effective radius as the half-light radius measured from growth curves. We do not take into account the PSF of the images, but this does not greatly affect our measurements because the measured radii are at least twice as large as the PSF. Uncertainties include contributions from both sky subtraction and measurement errors.

The circularised effective radius (r_e) of TX 0828+193 from the H_{160} image is 3.3±0.3 kpc, but the galaxy appears significantly smaller in the residual-H_{160} image with $r_e = 2.0 \pm 0.3$ kpc. A similar decrease in size is observed for MRC 0406-244, with $r_e = 4.4 \pm 0.3$ kpc measured from the H_{160} image, and $r_e = 2.9 \pm 0.3$ kpc measured from the residual-H_{160} image. Not taking into account the contribution

of the scattered quasar light and the nebular emission results in sizes that are approximately 65% larger than the true sizes of the red stellar population.

If the effective radii of the HzRGs are measured from the raw H_{160} images, then the HzRGs lie close to the mass-size relation of local galaxies. However, when we remove the nebular emission and scattered light, then the HzRGs lay below the relation for local galaxies, and have a similar mass-size relationship as other $z \sim 2$ galaxies (e.g. van de Sande et al. 2011).

6.3.4 Large-scale environment

HzRGs are frequently found within large overdensities of Lyα emitting galaxies (e.g. Venemans et al. 2007), indicating that many lie in forming protoclusters. Establishing protocluster association is more difficult for non-emission line galaxies. However, in a few cases, including the Spiderweb Galaxy, the excess of Lyα galaxies is found to be accompanied by an overdensity of red galaxies (Zirm et al. 2008), indicating a protocluster with an old galaxy population. No Lyα imaging is available for the MRC 0406-244 and TX 0828+193 fields, but the multicolour *HST* images allow us to search for an overdensity of red evolved galaxies.

The area-normalised $J_{110} - H_{160}$ colour distributions of the surrounding galaxies are shown in Fig. 6.4. For comparison we also plot the distribution of objects in the Spiderweb protocluster (labelled as 1138). To ensure that both the HzRG and control fields are at least 85% complete, we impose a magnitude cut of H = 26.

There is a marked difference between the density of red galaxies around, on the one hand MRC 0406-244 and TX 0828+193 and, on the other hand the Spiderweb galaxy. Although the uncertainties are large, the density of objects around MRC 0406-244 is not significantly different to that in the control field. The field around TX 0828+193 shows only a mild excess of objects with $J_{110} - H_{160} > 1.25$: the TX 0828+193 field is denser by a factor 1.7 ± 0.5, where the uncertainty is based on Poisson statistics. The strong difference with the Spiderweb protocluster observed at $J - H > 1.25$ cannot be due to selection effects since such a colour cut is slightly more efficient at selecting $z \sim 2.5$ galaxies than at selecting $z = 2.15$ galaxies. We therefore conclude that MRC 0406-244 and TX 0828+193 do not reside in protoclusters that are as dense in evolved galaxies as that around the Spiderweb galaxy.

The lack of evidence for a significant surface overdensity around 0406 and 0828, however, does not mean that these two fields do not host protoclusters. Following a similar argument as used in Kuiper et al. (2010), selecting high-z galaxies through a single near-infrared colour cut probes a large redshift range and therefore only a large volume overdensity can be detected as a significant surface overdensity. We therefore conclude that although we find no evidence that the large-scale environments of these HzRGs differ from that of other distant massive galaxies, the 0406 and 0828 fields may still host protoclusters. Narrowband imaging is needed to determine this.

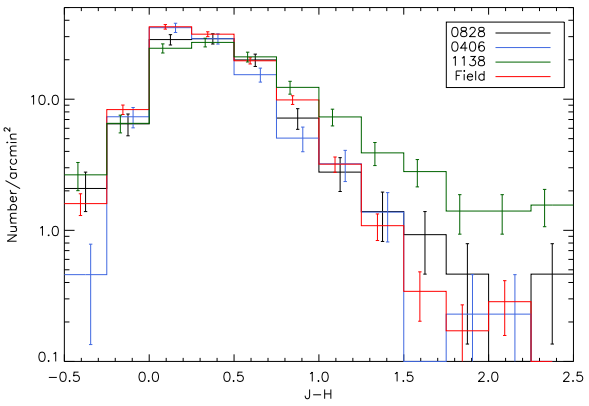

Figure 6.4 – Number of objects per unit area as a function of $J - H$ colour for all objects with $H < 26$ mag for the fields around TX 0828+193 (black), MRC 0406-244 (blue), the Spiderweb galaxy (1138; green), and the combined control fields (red). There is no sign of a significant overdensity of red galaxies in either of the radio galaxy fields.

6.4 Discussion

HzRGs are spectacularly beautiful galaxies, consisting of multiple clumps and filaments that extend tens of kpc from the galaxy core. Decomposing the light from MRC 0406-244 and TX 0828+193 shows that the nebular emission, scattered AGN light and young stars are aligned with the radio jets and contribute to the alignment effect, but that the red stellar population is not extended nor aligned with the young radio jets. Underneath all the AGN activity, these galaxies appear similar in size and environment to other distant massive galaxies. The red stellar population is located in a single central region, of similar size as sub-millimetre and other high redshift galaxies. It is just their short-lived AGN activity that places them in a league of their own. Once the AGN stops feeding, the jets, induced star formation and any associated winds will die down, and these galaxies may be difficult to distinguish from the rest of the massive galaxy population.

The extended light, however, does imply the presence of a large reservoir of cool and warm gas that extends tens of kpc from the radio galaxy. Nesvadba et al. (2008) estimate the ionised gas component is approximately 10^{10} $M_{\odot}$, however there is likely to be much more because AGN light is scattered off material in MRC 0406-244 that does not emit emission lines and the cool gas component is likely to be much larger. Does the large reservoir of material exist around all massive galaxies, and are these examples merely illuminated by the AGN activity, or are they a product of AGN outflows?

If these reservoirs are common to all distant massive galaxies, then maybe these will provide an answer concerning the existence of the undersized red galaxies observed at high redshift (e.g. Trujillo et al. 2007; Cimatti et al. 2008; van Dokkum et al. 2008, 2009). If a large, but unseen, gas reservoir is present around these galaxies then that might partially provide the increase in radius needed to put these extreme galaxies on the local size-mass relation. More work is needed to investigate whether this is a plausible scenario.

When comparing to the Spiderweb galaxy, we see that the Spiderweb galaxy shows several characteristics that suggest it is destined to evolve into a brightest cluster galaxy: it resides in one of the densest $z > 2$ protoclusters, is surrounded by tens of smaller galaxies that can be stripped to form an extended cD halo, and its mass of 10^{12} $M_{\odot}$ makes it one of the most massive galaxies at that redshift. MRC 0406-244 and TX 0828+193 are similar in appearance to the Spiderweb as they consist of several extended clumps which are aligned with the radio jets and are likely to be undergoing AGN feedback. However, neither MRC 0406-244 nor TX 0828+193 show as extreme behaviour as the Spiderweb galaxy: they contain only a fifth of the mass of the Spiderweb galaxy, there is no evidence that they lie in denser than average environments, and their immediate neighbourhood is not populated by many smaller galaxies which can form an extended cD halo. So whilst some HzRGs appear destined to become brightest cluster galaxies, the evolution and fate of TX 0828+193 and MRC 0406-244 is less clear and they may evolve to become more typical massive elliptical galaxies. All of these galaxies are undergoing powerful AGN feedback, that is sufficient to expel a significant fraction of the gas within their halos (Nesvadba et al. 2008). Thus, these AGN feedback phenomena neither require multiple galaxy mergers nor dense protocluster environments.

References

Bertin E., Arnouts S., 1996, A&AS, 117, 393
Bruzual G., Charlot S., 2003, MNRAS, 344, 1000
Chambers K. C., Miley G. K., van Breugel W., 1987, Nature, 329, 604
Cimatti A. et al., 2008, A&A, 482, 21
Croton D. J. et al., MNRAS, 365, 11
De Breuck C. et al., 2010, ApJ, 725, 36
Hatch N. A., Overzier R. A., Kurk J. D., Miley G. K., Röttgering H. J. A., Zirm A. W., 2009, MNRAS, 395, 114
Hatch N. A., Overzier R. A., Röttgering H. J. A., Kurk J. D., Miley G. K., 2008, MNRAS, 383, 931
Humphrey A., Iwamuro F., Villar-Martín M., Binette L., Fosbury R., di Serego Alighieri S., 2007, MNRAS, 382, 1729
Humphrey A., Iwamuro F., Villar-Martín M., Binette L., Sung E. C., 2009, MNRAS, 399, L34
Iwamuro F. et al., 2003, ApJ, 598, 178
Kuiper E. et al., 2010, MNRAS, 405, 969
Kurk J. D., Röttgering H. J. A. et al., 2000, A&A, 358, L1
McCarthy P. J., van Breugel W., Spinrad H., Djorgovski S., 1987, ApJ, 321, L29
Miley G., De Breuck C., 2008, A&A Rev, 15, 67
Miley G. K. et al., 2006, ApJ, 650, L29
Nesvadba N. P. H., Lehnert M. D., De Breuck C., Gilbert A. M., van Breugel W., 2008, A&A, 491, 407
Nesvadba N. P. H., Lehnert M. D., Eisenhauer F., Gilbert A., Tecza M., Abuter R., 2006, ApJ, 650, 693
Pentericci L., McCarthy P. J., Röttgering H. J. A., Miley G. K., van Breugel W. J. M., Fosbury R., 2001, ApJS, 135, 63
Pentericci L., Röttgering H. J. A., Miley G. K., McCarthy P., Spinrad H., van Breugel W. J. M., Macchetto F., 1999, A&A, 341, 329
Rush B., McCarthy P. J., Athreya R. M., Persson S. E., 1997, ApJ, 484, 163
Seymour N. et al., 2007, ApJS, 171, 353
Taniguchi Y. et al., 2001, ApJ, 559, L9
Targett T. A., Dunlop J. S., McLure R. J., Best P. N., Cirasuolo M., Almaini O., 2011, MNRAS, 412, 295
Trujillo I., Conselice C. J., Bundy K., Cooper M. C., Eisenhardt P., Ellis R. S., 2007, MNRAS, 382, 109
van de Sande J. et al., 2011, ApJ, 736, L9+
van Dokkum P. G. et al., 2008, ApJ, 677, L5
van Dokkum P. G., Kriek M., Franx M., 2009, Nature, 460, 717
Vanden Berk D. E., et al., 2001, AJ, 122, 549
Venemans B. P. et al., 2007, A&A, 461, 823
Vernet J., Fosbury R. A. E., Villar-Martín M., Cohen M. H., Cimatti A., di Serego Alighieri S., Goodrich R. W., 2001, A&A, 366, 7
Zirm A. W. et al., 2008, ApJ, 680, 224